THE JOURNAL OF BIOLOGICAL CHEMISTRY VOL. 287, NO. 43, pp. 36536–36543, October 19, 2012

Resolving the Negative Potential Side (n-side) Water-accessible Proton Pathway of F-type ATP Synthase by Molecular Dynamics Simulations*

Received for publication, July 6, 2012, and in revised form, August 20, 2012 Published, JBC Papers in Press, August 31, 2012, DOI 10.1074/jbc.M112.398396

Holger Gohlke[‡1], **Daniel Schlieper**[§1], **and Georg Groth**[§2]

From the [‡]*Institute of Pharmaceutical and Medicinal Chemistry and* [§]*Institute of Biochemical Plant Physiology, Heinrich Heine University, 40204 Düsseldorf, Germany*

Background: ATP synthase converts a transmembrane gradient of protons or Na^+ into chemical energy.
Results: Molecular dynamics simulations mapped a water half-channel as part of the proton path.
Conclusion: The half-channel is inclined against the sense of rotation of the *c*-ring, minimizing futile proton flow.
Significance: The geometry of the proton path is crucial in understanding the energy coupling of ATP synthase.

The rotation of F_1F_o-ATP synthase is powered by the proton motive force across the energy-transducing membrane. The protein complex functions like a turbine; the proton flow drives the rotation of the *c*-ring of the transmembrane F_o domain, which is coupled to the ATP-producing F_1 domain. The hairpin-structured *c*-protomers transport the protons by reversible protonation/deprotonation of a conserved Asp/Glu at the outer transmembrane helix (TMH). An open question is the proton transfer pathway through the membrane at atomic resolution. The protons are thought to be transferred via two half-channels to and from the conserved *c*Asp/Glu in the middle of the membrane. By molecular dynamics simulations of *c*-ring structures in a lipid bilayer, we mapped a water channel as one of the half-channels. We also analyzed the suppressor mutant *c*P24D/E61G in which the functional carboxylate is shifted to the inner TMH of the *c*-protomers. Current models concentrating on the "locked" and "open" conformations of the conserved carboxylate side chain are unable to explain the molecular function of this mutant. Our molecular dynamics simulations revealed an extended water channel with additional water molecules bridging the distance of the outer to the inner TMH. We suggest that the geometry of the water channel is an important feature for the molecular function of the membrane part of F_1F_o-ATP synthase. The inclination of the proton pathway isolates the two half-channels and may contribute to a favorable clockwise rotation in ATP synthesis mode.

ATP synthases from bacteria, mitochondria, and chloroplasts produce ATP, the universal fuel in biological cells. To synthesize the high energy triphosphate from ADP and inorganic phosphate, the enzymes use a transmembrane proton gradient (1–4) and convert electrochemical into chemical energy. F-type ATP synthases consist of a transmembrane F_o domain and an extramembranous F_1 domain. F_o from chloroplasts comprises a rotating *c*-ring and a stator domain formed by subunits *a*, *b*, and *b*′. Although the stoichiometry of the transmembrane stator domain is fixed in all organisms, the *c*-ring has 8 subunits in bovine mitochondria (5), 10 subunits in yeast mitochondria (1), 14 subunits in chloroplasts (6, 7), and 10–15 subunits in bacteria (8–15). The chloroplast F_1 domain comprises subunits γ and ϵ, which rotate with the *c*-ring, and the nonrotating catalytic domain $\alpha_3\beta_3$, which is connected to the stator domain of F_o through the δ subunit (see Fig. 1*A*). Light-driven proton pumps in chloroplasts and phototropic bacteria or respiratory-chain enzymes in mitochondria and aerobic bacteria generate a proton gradient across the membrane, resulting in a positively charged p-side[3] and a negatively charged n-side (p-side and n-side refer to lumen and stroma in chloroplasts, intermembrane space and matrix in mitochondria, and periplasm and cytoplasm in bacteria, respectively). The resulting proton motive force drives the $c_{8-15}\gamma\epsilon$ rotor, which induces conformational changes in the β subunits of the stator and, hence, provides the energy to produce ATP. Some fermenting bacteria use sodium ions instead of protons to drive ATP synthesis (16).

Subunits *a* and *c* of the transmembrane F_o domain are directly involved in proton transport. Transport from the p-side to the middle of the membrane where protons bind to a conserved carboxylate of subunit *c* (Glu^{61} in chloroplasts) is facilitated by an intrinsic channel or proton wire in subunit *a* (p-side half-channel) (17–22). Protonation of the essential carboxylate in the *c*-subunit drives clockwise rotation of the entire *c*-ring (as seen from the p-side) (23). The step size of the *c*-ring corresponds to one subunit of *c*, indicating a proton motive force-driven Brownian ratchet mechanism (24, 25). The protons are then released from the proton-binding site on subunit *c* to the n-side (17, 26). An aqueous path at the interface between subunits *a* and *c* was inferred by mutagenesis and

* This work was supported by a grant from the Deutsche Forschungsgemeinschaft (GR 1616/5-3) (to G. G.) and by funds of the initiative "Fit for Excellence" at the Heinrich Heine University (to H. G.).
[1] Both authors contributed equally to this work.
[2] To whom correspondence should be addressed. Tel.: 49-211-811-1288; Fax: 49-211-811-3569; E-mail: georg.groth@hhu.de.

[3] The abbreviations used are: p-side, positive side of the membrane; n-side, negative side of the membrane; MD, molecular dynamics; NPAT, constant area isobaric-isothermal ensemble; NPT, isobaric-isothermal ensemble; NVT, canonical ensemble; r.m.s.d., root mean square deviation(s); TMH, transmembrane helix; PDB, Protein Data Bank.

labeling studies (18, 19, 21, 27–29), which may function as the n-side half of the proton channel. F_1F_o-ATP synthases can also catalyze the reverse reaction driven by ATP hydrolysis and pump protons from the n-side to the p-side of the membrane via the same half-channels, resulting in a counterclockwise rotation of the *c*-ring rotor (23).

Preventing a nonproductive shortcut between the p-side and the n-side half-channels is an essential prerequisite for the transformation of proton flux into mechanical energy (26). A conserved positively charged side chain in subunit *a* (Arg^{193} in chloroplasts and Arg^{210} in *Escherichia coli*) isolates the two half-channels by preventing any protonated (and thus uncharged) Glu^{61} of subunit *c* to pass the positively charged guanidinium group of the $aArg^{193}$ side chain (30–35). Thus, $aArg^{193}$ prevents the futile counterclockwise rotation in ATP synthesis mode.

However, the structure of the *a/c* interface and how the protein complex maintains isolation between the half-channels, *i.e.* how the nonrotating shortcut of protons is prevented, has remained elusive so far. Although it is established that the n-side half-channel is water-accessible, the pathway of the protons has not yet been identified. Here we resolve this pathway at atomic resolution by MD simulations of the structure of the c_{14} rotor ring of the chloroplast ATP synthase (7) in a lipid bilayer surrounded by water. The carboxylate $cGlu^{61}$ of one of the protomers was deprotonated, thus mimicking the protomer facing the *a* subunit in the intact F_o domain. We identified a water-accessible region inside the lipid bilayer at the periphery of the *c*-ring rotor. This water channel runs from the n-side of the membrane to the deprotonated carboxylate $cGlu^{61}$ in the middle of the membrane. The aqueous n-side half-channel is not parallel to the axis of the *c*-ring rotor but rather inclined, which may enhance the isolation between the half-channels and may contribute to a favorable clockwise rotation in ATP synthesis mode. The MD results also give a plausible explanation of the peculiar properties of the double mutant *c*P24D/E61G, which, in *E. coli*, is fully functional despite lacking the essential Asp^{61} side chain (36); the water channel now reaches deep between two *c*-protomers, thus enabling the repositioning of the reversibly protonated carboxyl group of the suppressor mutant.

EXPERIMENTAL PROCEDURES

Generation of c_{14} Rotor Ring/Lipid Bilayer Starting Structures—Starting structures for MD simulations of the c_{14} rotor ring in a membrane environment were generated from the crystal structure of the *c*-ring from spinach chloroplasts (Protein Data Bank (PDB) code 2w5j) (7). It comprises 14 identical *c*-subunits, each of which forms a hairpin structure consisting of two TMHs. Missing amino acids and side chains were added manually in the most plausible rotamer conformations and refined as described (7). The *c*-ring structure was oriented with respect to a lipid bilayer according to information provided by the Orientations of Proteins in Membranes database (37). The protein structure was then embedded in a bilayer of 288 1,2-dioleoyl-*sn*-glycero-3-phosphorylcholine lipids, which itself was embedded in 20 Å layers of water molecules above and below. The pre-equilibrated configuration of the lipid bilayer and the water layers was taken from Rosso and Gould (38). Ninety-nine lipids that were sterically overlapping with the protein structure were removed. The center of the *c*-ring was filled with 12 lipids to model the lipid plug seen in isolated rings (39).

From this system, the following starting structures were generated. I) All but one of the Glu^{61} residues of the subunits *c* were protonated (hitherto referred to as "13protonated"). II) All Glu^{61} residues were protonated ("14protonated"). III) All Glu^{61} residues were deprotonated ("0protonated"). IV) The double mutant *c*P24D/E61G was generated by pruning the side chain of Glu^{61} and replacing Pro^{24} with the most plausible rotamer of Asp, as provided by Coot (40). In this system, all but one of the Asp^{24} residues were then protonated (double mutant). To reach electroneutrality for each of these starting structures, sodium ions were added by the leap program of the Amber package (41) as required. This resulted in system sizes of ~78,000 atoms.

Molecular Dynamics Simulations—MD simulations were performed with the Amber 10 suite of programs (41). For the protein and ions, the force field by Cornell *et al.* (42) was used with modifications suggested by Simmerling *et al.* (43). TIP3P was used as a water model (44). For the lipids, force field parameters and charges derived by Rosso and Gould (38) were used, which are based on the General Amber Force Field (45) and the RESP procedure (46), respectively. These parameters have been shown to yield area per lipid values, peak distances, and lipid volumes that converge around values close to experimental ones when simulations were performed under the condition of an isobaric-isothermal ensemble (NPT) with anisotropic pressure control (38). That way, a restraining of the area as in a constant area isobaric-isothermal (NPAT) ensemble can be avoided, which may lead to simulation artifacts (47).

Accordingly, after minimization of the systems for 2000 steps with the protein atom positions restrained, canonical ensemble (NVT) MD was carried out for 50 ps, during which the system was heated from 100 to 300 K, applying harmonic restraints with force constants of 5 kcal mol^{-1} $Å^{-2}$ to the protein atoms. Subsequent NPT-MD was used for 150 ps to adjust the density. After gradually reducing the force constants of the harmonic restraints on solute atom positions to zero during 250 ps of NPT-MD, the following 20 ns of NPT-MD at 300 K were used to further equilibrate the system. Equilibration times of this length were shown to be necessary for typical simulation studies involving lipid bilayers (48). Finally, the following trajectories of 30 ns length generated by NPT-MD were used as production runs with conformations extracted every 20 ps. This resulted in ~250 ns of total simulation time.

Throughout the simulations, the particle mesh Ewald method (49) was used to treat long-range electrostatic interactions, and bond lengths involving bonds to hydrogen atoms were constrained using SHAKE (50). The time step for all MD simulations was 2 fs, with a direct space, nonbonded cutoff of 8 Å. The temperature was controlled using the Berendsen thermostat (51) with a time constant of 10 ps, and the Berendsen barostat (51) was used for anisotropic pressure control with a time constant of 2 ps.

Analysis of the Production Runs—The production runs were analyzed with ptraj of the Amber suite of programs (41). The "watershell" command was used for analyzing the first and second solvation shells with respect to the oxygen atoms of Glu^{61} (13protonated, 14protonated, 0protonated) or of Asp^{24} (double mutant) using lower and upper distances of 3.4 and 5.0 Å, respectively. Water densities were determined with the "grid" command using a cubic grid that encompasses the whole simulation cell with a spacing of 1 Å in each direction. Depicted contour surfaces encompass regions with at least 50 counts of water molecules over the 1,500 snapshots analyzed. Prior to calculating root mean square deviations (r.m.s.d.) and an average structure, the *c*-ring structure was superimposed with respect to all C_α atoms. A snapshot with a minimal C_α atom r.m.s.d. to the average structure was then taken as the representative structure depicted in Figs. 1 and 2. χ_1 and χ_2 angles of residues Glu^{61} were determined as the torsion angles involving atoms N-C_α-C_β-C_γ and C_α-C_β-C_γ-C_δ, respectively. The kink of the outer helices of the *c*-ring was determined as the angle of the point triple (center of mass of C_α atoms of residues 48–50; C_α atom of residue 61; center of mass of C_α atoms of residues 74–76). The S.E. was determined as the S.D. divided by the square root of the number of independent snapshots. The number of independent snapshots was determined from the time correlation function for the respective analysis. The correlation time was 200 ps in the case of the watershell analysis and 2.2 ns in the case of the analysis of the χ_1 and χ_2 torsion angles of Glu^{61}.

To analyze possible conformational changes of the *c*-ring, an elastic network model analysis was performed with the ElNémo webserver (52) using default parameters. Molecule figures were prepared with PyMOL (Schrödinger, New York, NY).

RESULTS

We performed MD simulations of 50 ns length of the chloroplast c_{14}-ring in an aqueous lipid bilayer with Na^+ counter ions, with the last 30 ns taken for analysis. Although the conserved Glu^{61} side chain from 13 protomers was protonated, the carboxyl group of one Glu^{61} was deprotonated and thus charged (13protonated). This situation reflects the physiological condition of the *c*-ring in active ATP synthase where aArg^{189} serves as counter ion. The water density was determined by counting the presence of water molecules within a cubic grid of 1 Å spacing. Fig. 1 shows an MD snapshot with a minimal r.m.s.d. to the average protein structure together with the water density as seen from the top, front, and side (Fig. 1, *B*, *C*, and *D*, respectively). Although no water was present inside the 1,2-dioleoyl-*sn*-glycero-3-phosphorylcholine membrane at the start of the calculation, a water channel developed during the simulation originating from the n-side and reaching to the middle of the membrane bilayer, enclosing the deprotonated Glu^{61} with its tip (Table 1).

We mapped the wetted surface on the *c*-ring conformation with a minimal r.m.s.d. to the average structure (Fig. 2*A*). The main amino acids in contact with the water channel are listed in Table 2. This water channel is in agreement with experimental data that implied a water-accessible region in the interface between subunits *a* and *c* (18, 19, 21, 27–29). We also performed an MD simulation of a *c*-ring with Glu^{61} of all 14 protomers protonated (14protonated) and of a completely deprotonated *c*-ring (0protonated). No water channel developed with the protonated (uncharged) *c*-ring (Fig. 2*B*; Table 1). In contrast, with the fully deprotonated and therefore charged *c*-ring, the water encompassed almost completely the n-side half of the *c*-ring (Fig. 2*C*; Table 1).

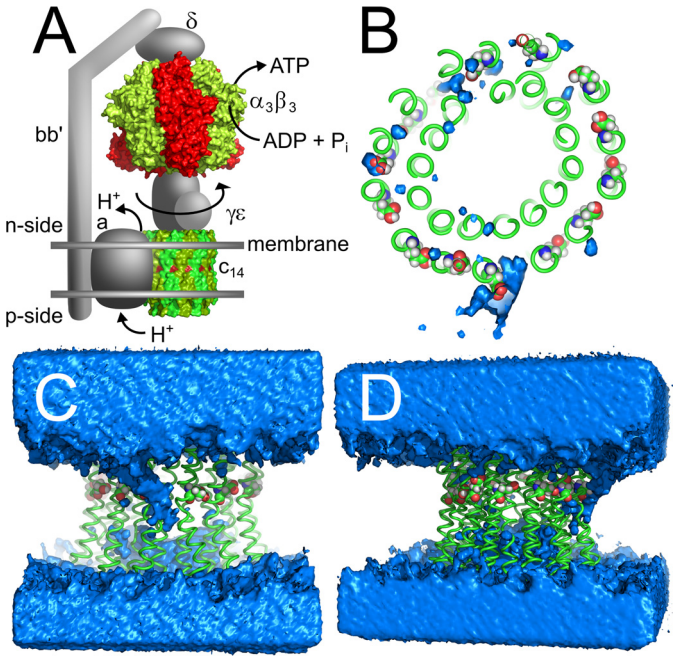

FIGURE 1. **Chloroplast ATP synthase.** *A*, current model using the x-ray structures of $\alpha_3\beta_3$ (PDB code 1KMH) (67) and c_{14}-ring (PDB code 2W5J) (7). Protons flow from the p-side (lumen) through subunit *a* to the n-side (stroma) and drive the rotation of subunits $c_{14}\gamma\epsilon$. This rotation induces ATP synthesis in the β subunits. Subunits *b* and *b'* provide a stator stalk between subunits *a* and $\alpha_3\beta_3\delta$. *B*, top view; *C*, front view; *D*, side view depicting the water channel found in the MD simulation of the 13protonated system. *Blue*, water density at a contour level of 50 waters/Å^3 during the course of the simulation. *Green*, backbone of c_{14}-ring. *Red*, oxygen atoms of conserved Glu^{61}. The lipid bilayer is omitted for clarity. *A*, *C*, and *D*, *top*, n-side, and *bottom*, p-side.

Suppressor Mutant cP24D/E61G—We also performed an MD simulation of the suppressor mutant *c*P24D/E61G, in which the carboxyl group of one Asp^{24} was deprotonated and thus charged. In this mutant, the function of the reversibly protonated carboxyl group of conserved Glu^{61} (Asp^{61} in *E. coli*) is transferred from the outer *c*TMH2 to Asp^{24}, which is located on the adjacent inner *c*TMH1 (36). Fig. 2, *D*–*F*, show the resulting water density maps over the last 30 ns of the trajectory together with the closest-to-average conformation of the *c*-ring. As with the wild type *c*-ring, a water channel developed and reached as far as the carboxylate group of Asp^{24} (Table 1).

Structural Changes of the c-Ring—Regarding possible structural changes of subunit *c* upon deprotonation, we do not observe significant differences between the protomer with deprotonated Glu^{61} and the other, protonated protomers for the 13protonated system. In fact, the overall C_α atom r.m.s.d. remains stable below 4 Å over the trajectory, and the C_α atom r.m.s.d. of almost all TMHs remains below 3 Å. Furthermore, the kink of TMH2 of subunit *c*, which gives the *c*-ring the characteristic hourglass shape, is essentially the same; the kink angle of the helix with deprotonated Glu^{61} is 158.7° ± 1.0° (S.E.),

TABLE 1

Number of water molecules around reversibly protonated amino acid side chains

Average ± S.E. of the number of water molecules within 3.4 and 5 Å over the MD trajectories from 20 to 50 ns.

Name	Protonation state	Amino acid	3.4 Å shell	5 Å shell
13protonated	13 neutral +1 charged	Deprotonated Glu^{61}	5.41 ± 0.20	8.16 ± 0.38
		Protonated Glu^{61}	0.28 ± 0.01	0.92 ± 0.21
14protonated	14 uncharged	Protonated Glu^{61}	0.90 ± 0.03	0.58 ± 0.21
0protonated	14 charged	Deprotonated Glu^{61}	5.12 ± 0.05	10.97 ± 0.10
Double mutant	P24D/E61G (13 + 1)	Deprotonated Asp^{24}	3.10 ± 0.12	4.28 ± 0.35
		Protonated Asp^{24}	0.44 ± 0.19	1.23 ± 0.41

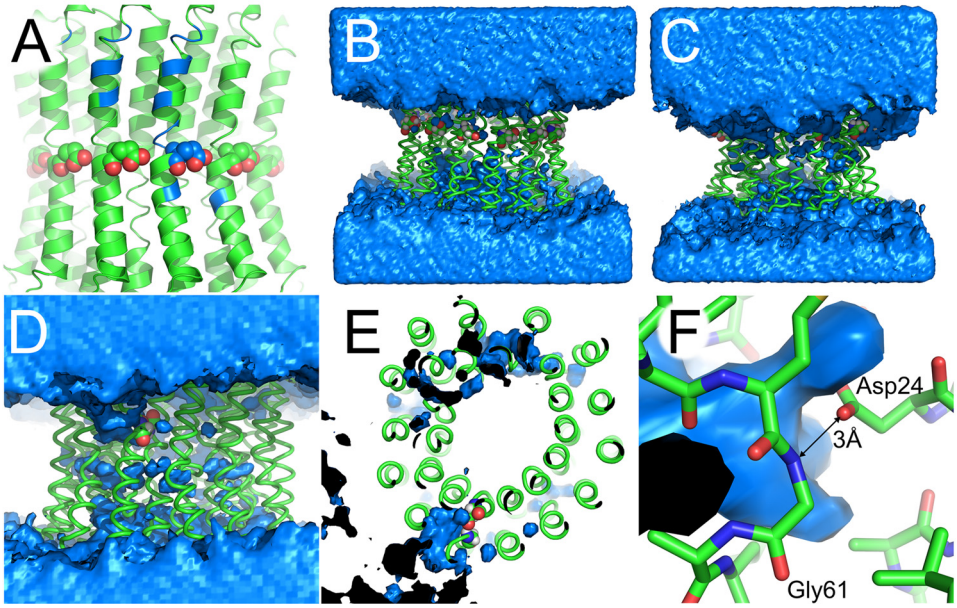

FIGURE 2. **The water channel in different simulations.** The lipid bilayer is omitted for clarity. *A*, map of the water channel from Fig. 1 on the starting structure. *Blue*, main amino acids in contact with the water channel (see Table 2 for a list). *B* and *C*, comparison of water distribution in control MD simulations. *B*, *c*-ring with Glu^{61} of all 14 protomers protonated (uncharged). *C*, *c*-ring with all Glu^{61} deprotonated. Although the protonated ring (*B*) does not show a distinct water channel, a water ring is drawn toward the charged center of the *c*-ring (*C*). *D–F*, water channel in suppressor mutant *c*P24D/E61G. *D*, front view. The water channel developed from the top (n-side) to the one charged Asp^{24}. This channel is inclined to the vertical membrane normal and runs, as depicted here, from the *top left* to the *center*. *E*, top view. The water channel reaches as far as the carboxylate group of Asp^{24}. *F*, close-up view. The carboxylate group of Asp^{24} establishes a hydrogen bond with the amide nitrogen of Gly^{61} with a distance of 3 Å. Gln^{28} is hidden for clarity. *A–D* and *F*, *top*, n-side; *bottom*, p-side. *A–C*, *spheres* show Glu^{61} of *c*-protomers. *D–F*, *spheres* show *c*Asp^{24}. *B–F*, *blue*, water density at a contour level of 50 waters/$Å^3$ over the course of the simulation. *Black*, inside of water density.

TABLE 2

Main amino acids in contact with the water channel

Listed are amino acids close to the water channel as mapped in Fig 2*A*. The *c*-protomer with the deprotonated Glu^{61} is denoted *n*. During ATP synthesis, the protomers to the left (in the orientation of Fig. 1A) are the next to be rotated into proton release position and are thus numbered *n*−1 and *n*−2. Accordingly, the protomer to the right is denoted *n*+1.

Protomer	Amino acid
n−2	Glu^{46}
n−1	Glu^{46}, Gly^{47}, Arg^{50}, Gly^{51}, Leu^{54}
n	Glu^{46}, Gly^{47}, Lys^{48}, Arg^{50}, Gly^{51}, Leu^{55}, Ala^{58}, Phe^{59}, Met^{60}, Glu^{61}, Ile^{65}
n+1	Tyr^{66}

whereas the average of 11 protonated helices is 159.7° ± 0.8°. In the latter case, the two protomers adjacent to the helix with the deprotonated Glu^{61} have been excluded to prevent a possible influence of the deprotonated protomer. The circular shape of the *c*-ring got distorted during the MD simulations (Fig. 1*B*). The degree and direction of distortion are consistent with results from an elastic network model analysis. This analysis reveals that the first four low frequency modes lead to a deformation of the *c*-ring structure perpendicular to the axis of the *c*-ring rotor; the first two of these modes preferentially distort the p-side of the *c*-ring, the last two distort the n-side (data not shown). In each case, the distorted structures take on an oval shape. A similar distortion, although to a lesser degree, has been observed in electron micrographs from *Ilyobacter tartaricus* (53). Finally, visual inspection of the trajectories showed no swiveling motion of the helices (data not shown).

Glu^{61} Side Chain Conformation—Proton binding of Glu^{61} is linked to a conformational change of this amino acid (7, 54, 55). We analyzed the conformations of Glu^{61} according to the torsion angles χ_1 and χ_2 and classified the conformations as *plus*, *trans*, and *minus* according to Lovell *et al.* (56). Torsion angle χ_1 of the deprotonated Glu^{61} adopts values of around −65° (*minus*) and around −177° (*trans*), whereas torsion angle χ_2 is mostly *trans* (Fig. 3*A*). Overall, the all-*trans* rotamer is mostly populated where the side chain points to the solvent. This finding agrees with the observation of an extended conformation of Glu^{59} in the deprotonated *c*-ring from yeast (55). The protonated side chains have similar χ_1 torsion angles with *minus* and *trans* conformations and similar χ_2 torsion angles in *minus* and *trans* conformations. However, the *plus* conformation of χ_2 is populated, too (Fig. 3*B*). Overall, this leads to the *trans*/*plus*

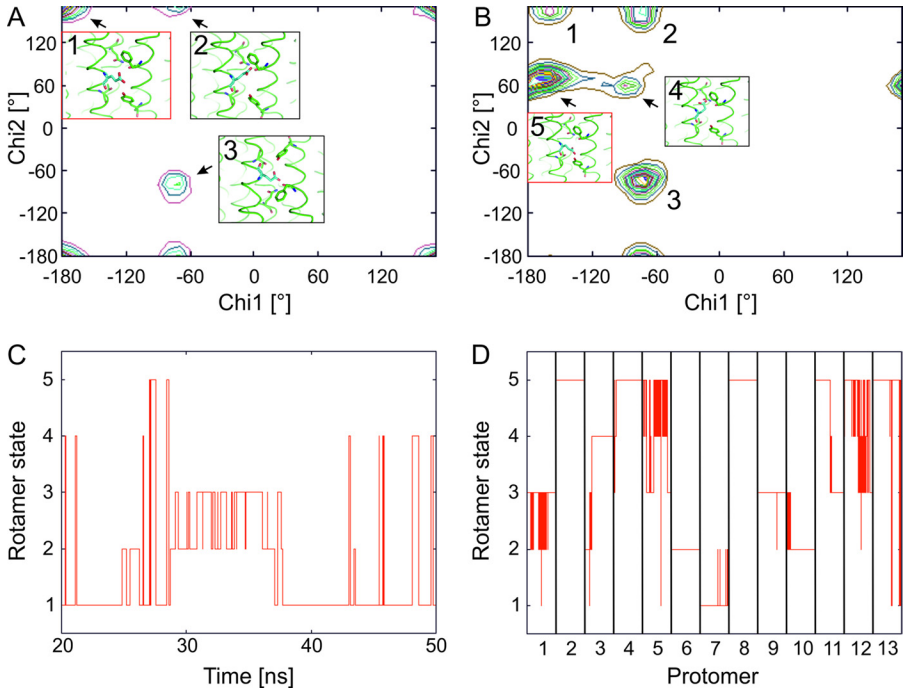

FIGURE 3. **Rotamer states of the side chain of Glu^{61} from the MD simulation of the 13protonated system.** *A* and *C*, states of deprotonated (charged) Glu^{61} rotamers. *B* and *D*, states of protonated (uncharged) Glu^{61} rotamers. *A*, distribution of rotamer states according to the χ_1/χ_2 map. The number of rotamer states is qualitatively indicated by 20 equally spaced contour lines. The *insets* show the most abundant rotamer states 1–3 with 1 being the most populated one (*red frame*). *B*, distribution of rotamer states according to the χ_1/χ_2 map. The *insets* show the two rotamer states not observed for the deprotonated Glu^{61} (see *panel A*). Rotamer 5 is the most populated one (*red frame*). *C*, transitions between rotamer states along the trajectory. *States 1–3* correspond to the ones shown in *panel A*; rotamer *states 4* and *5* are lowly populated and, hence, not shown in *panel A*. *D*, transitions between rotamer states along the trajectory for each of the 13 protomers. *States 1–5* correspond to the ones shown in *panel B*. Each column represents a trajectory from 20–50 ns.

rotamer being most abundant, with the side chain pointing inward toward Gln^{28}. On multiple occasions during the MD simulation, transitions between rotamer states of Glu^{61} occur (Fig. 3, *C* and *D*) for both the deprotonated Glu^{61} and the protonated ones, showing a pronounced mobility of these side chains.

DISCUSSION

A major challenge in understanding the molecular mechanism of energy coupling in the F_1F_o-ATP synthase is to resolve the proton transfer pathway in the transmembrane F_o domain at atomic resolution. Currently, there are only two cryo-electron microscopy structures of F_o subcomplexes available. The first structure is from *Thermus thermophilus* ATP synthase with 10 Å resolution (57). Here, subunit *I* (the functional homolog of subunit *a*) forms two complete half-channels from eight TMHs that are thought to be offset laterally. The other available structure is the ab_2c_{11} F_o subcomplex of the Na^+-translocating F-ATP synthase from *I. tartaricus* with 7 Å resolution (53). Here, subunit *a* forms one four-helix bundle that probably provides the p-side half-channel. Additionally, up to three more TMHs, which belong to subunit *a* and perhaps subunit *b*, can be seen in the electron density. Subunits *a* of ATP synthases from *E. coli* or chloroplasts comprise five TMHs (58, 59), and a water channel serves as the n-side half-channel (18, 19, 21, 27–29). Hence, the F_o subcomplexes from *E. coli*, chloroplasts, and *I. tartaricus* may share the same architecture. The current model of the active ATP synthase (3) predicts that one protomer of subunit *c* has the conserved acidic side chain (Glu^{61} in chloroplast ATP synthase) deprotonated. Its charge is neutralized by *a*Arg^{189}. The remaining *c*-protomers (13 in chloroplasts) have protonated Glu^{61} and are embedded in the hydrophobic part of the membrane. To reflect this situation in our MD calculations, our starting model of the spinach chloroplast *c*-ring rotor was set to an ensemble of 13 protonated *c*-protomers plus one deprotonated *c*-protomer. This complex was embedded in a lipid bilayer enclosed by water layers. Although *c*-protomers are unlikely to be charged outside the *a/c* interaction, the MD simulation of this setting provides an elegant way to investigate possible structural changes that result from deprotonation of one *c*-protomer. We predicted earlier that for proton translocating ATP synthases, the conformational differences between protonated and deprotonated protomers are mainly limited to side chain movements of Glu^{61} (7), as is probably the case with Na^+-translocating ATP synthases (60). This model was later confirmed with a high resolution structure of ATP synthase from cyanobacterium *Spirulina platensis* (54).

Our MD simulations presented here do support the idea that the main conformational changes of a protomer upon deprotonation are limited to the side chain movements of Glu^{61}. The trajectories show no indication of helix swiveling, nor other major changes in helix conformation. Transitions between rotamer states in our simulation reveal a certain mobility of the side chains of both the protonated Glu^{61} and the deprotonated Glu^{61}. This observed mobility of the side chain in the hydrophobic part of the membrane moderates the stringent implication of the description of a "locked conformation" for protonated Glu^{61} (60).

The most striking result from our MD simulations is the location of water molecules inside the hydrophobic part of the lipid bilayer forming a water channel. The existence of a water channel has been extensively shown by *in vitro* experiments using chemical modification of *c*-rings with Cys substitutions (28, 29). Previous MD simulations also found water molecules drawn into the membrane. However, these simulations used *c*-rings with all Glu^{61} deprotonated (equivalent to our 0protonated system) (55, 61), and a complete water ring was formed. Other simulations used *c*-rings with a single protomer deprotonated (equivalent to our 13protonated system), but the authors missed to observe a distinct water channel (61, 62). The form and direction of the water channel identified here are instructive because the channel is not perpendicular to the membrane but points at an angle of ~45° from the n-side of the membrane to $cGlu^{61}$ and beyond. Therefore, the resulting proton wire does not follow the shortest path from $cGlu^{61}$ to the n-side but points against the rotational sense of the *c*-ring (in ATP synthesis mode). This orientation isolates the protons arriving from the p-side at the *c*-ring and the protons leaving from the *c*-ring to the n-side. As a result, two laterally offset half-channels are formed as proposed (3, 4) and seen in *T. thermophilus* ATP synthase (57), but with the difference that the n-side half-channel in the case of chloroplast ATP synthase is a hydration layer in the *a/c* interface as depicted in Fig. 2*A*. The orientation can also be expected to favor deprotonation of Glu^{61} on rotating from the position at protomer $n-1$ to the one at protomer n due to the presence of a higher dielectric environment that better stabilizes the emerging charge than a pure lipid environment. Accordingly, one may speculate that the orientation of the water channel contributes to a favorable clockwise rotation in ATP synthesis mode.

Control Calculations—Two additional MD simulations were performed to test the notion that a water channel is drawn into the hydrophobic part of the membrane if $cGlu^{61}$ is deprotonated and thus charged. With a fully protonated *c*-ring, less than 0.6 waters are found within 5 Å of the carboxyl group of Glu^{61} (Table 1). The fully deprotonated *c*-ring provides the opposite setting, where nearly 11 waters are found in the 5 Å shell (Table 1). Comparison of the water densities shows that the water did not integrate into the membrane with the fully protonated complex, whereas with the fully deprotonated complex, a complete water ring developed from the n-side to the center of the membrane (Fig. 2, *B* and *C*). Thus, these results confirm that the charged Glu^{61} in the hydrophobic part of the membrane leads to water molecules hydrating the protein/lipid interface.

Implications on an a/c Interface Model—As was argued earlier (62), *c*-protomers are not likely to be deprotonated outside the *a/c* interface. Here, we take full advantage of the possibility to simulate a functional state of the *c*-ring with one deprotonated and 13 protonated protomers in MD calculations. We predict that the resulting water channel shows a negative imprint of the hydrated *a/c* interface. This prediction is in line with findings from the *E. coli* subunit *a*. I) *a*TMH4 is positioned next to the outer TMH of *c* (63). II) This helix is kinked at the conserved Gly^{213}, as shown by NMR experiments on site-directed paramagnetic spin-labeled protein (64). III) According to the topology established with vesicles (58) and with *a/c* fusion proteins (65), *a*TMH4 is oriented with the N terminus on the n-side and the C terminus on the p-side. IV) The 15 amino acids preceding the conserved Arg^{210} are inaccessible to surface labeling (66). Therefore, it is feasible that the p-side half of *a*TMH4, *i.e.* the first 15 amino acids up to the conserved Arg^{210} (*E. coli* numbering), forms a straight helix from the p-side to the middle of the membrane. This part of the helix is probably parallel to the rotational axis of the *c*-ring. The helix is kinked at Gly^{213} and probably follows the direction of the water channel to the n-side. A layer of water molecules at the protein-protein interface provides the n-sided proton half-channel.

The proton-providing half-channel on the p-side is thought to be within subunit *a*, presumably inside a four-helix bundle (19, 20, 53). We predict that the location of this four-helical bundle is offset by one *c*-protomer from the n-sided water channel. As a result of the model, two *c*-protomers may be deprotonated simultaneously: one protomer with Glu^{61} in the water channel, releasing a proton, and one protomer with Glu^{61} interacting with conserved $a Arg^{189}$ ($a Arg^{210}$ in *E. coli*). This prediction is in accordance with the observation that in *T. thermophilus* ATP synthase, two four-helix bundles of subunit *I* are seen in the interface with the rotor (57).

Double Mutant—We modeled the suppressor mutant *c*P24D/E61G. In this variant, the reversibly protonated carboxylate is transferred from Glu^{61} in *c*TMH2 to position 24 in the adjacent helix of the *c* hairpin. *E. coli* cells with this double mutant grow via oxidative phosphorylation (36). The ATP synthase complex with this suppressor mutant actually produces ATP (although slightly less efficiently) and is resistant to dicyclohexylcarbodiimide, a potent inhibitor of wild type *c*-ring (36). Our MD simulation shows that water is drawn deep into the protein structure to the carboxylate group of deprotonated Asp^{24} (Fig. 2, *D–F*). Presumably, here at the interface between *c*TMH1 and *c*TMH2 is where the protons are bound. Thus, the water channel allows the protons to be released from a different position than in wild type. Its location in the inner interface of the hairpin-structured *c*-protomer may render the mutant insensitive to dicyclohexylcarbodiimide. In this simulation, the water channel is oriented in an angle against the rotational sense, too (*i.e.* in Fig. 2*D*, from the *upper left* to the *center*). The water channel is narrower than with wild type protein (Table 1), which may explain why the mutant is less efficient. Our model may also explain why Gly^{61} is essential for this double mutant; the side chain of Asp^{24} is likely to form a hydrogen bond with the nitrogen atom of Gly^{61} with an O → N distance of ~3 Å (Fig. 2*E*), which may be prevented by C_β of any other amino acid in position 61.

Conclusion—The MD simulations presented here give a convincing picture; the charges of $a Arg^{198}$ and $cGlu^{61}$ provide a strong driving force for water to move into the *a/c* interface, which is known to be hydrated at the n-side (18, 19, 21, 27–29). The surface of subunit *c*, and presumably also of subunit *a*, orients this water channel at an angle to the membrane normal. This water channel forms a proton path that is partially directed against the rotational sense of the *c*-ring (in ATP synthesis mode). Therefore, the hydrated proton path on the n-side is laterally offset to the p-side path, which presumably is inside a

four-helix bundle in subunit *a*. This geometry promotes isolation between half-channels minimizing futile proton flow and is suggested to contribute to a favorable clockwise rotation in ATP synthesis mode.

Acknowledgments—We thank the Heinrich Heine University Center for Information and Media Technology for computational support and Elisabeth Stratmann for assisting with the manuscript.

REFERENCES

1. Stock, D., Leslie, A. G., and Walker, J. E. (1999) Molecular architecture of the rotary motor in ATP synthase. *Science* **286,** 1700–1705
2. von Ballmoos, C., Wiedenmann, A., and Dimroth, P. (2009) Essentials for ATP synthesis by F_1F_0 ATP synthases. *Annu. Rev. Biochem.* **78,** 649–672
3. Junge, W., Sielaff, H., and Engelbrecht, S. (2009) Torque generation and elastic power transmission in the rotary F_OF_1-ATPase. *Nature* **459,** 364–370
4. Vik, S. B., and Antonio, B. J. (1994) A mechanism of proton translocation by F_1F_0 ATP synthases suggested by double mutants of the *a* subunit. *J. Biol. Chem.* **269,** 30364–30369
5. Watt, I. N., Montgomery, M. G., Runswick, M. J., Leslie, A. G., and Walker, J. E. (2010) Bioenergetic cost of making an adenosine triphosphate molecule in animal mitochondria. *Proc. Natl. Acad. Sci. U.S.A.* **107,** 16823–16827
6. Seelert, H., Poetsch, A., Dencher, N. A., Engel, A., Stahlberg, H., and Müller, D. J. (2000) Proton-powered turbine of a plant motor. *Nature* **405,** 418–419
7. Vollmar, M., Schlieper, D., Winn, M., Büchner, C., and Groth, G. (2009) Structure of the c_{14} rotor ring of the proton translocating chloroplast ATP synthase. *J. Biol. Chem.* **284,** 18228–18235
8. Jiang, W., Hermolin, J., and Fillingame, R. H. (2001) The preferred stoichiometry of *c* subunits in the rotary motor sector of *Escherichia coli* ATP synthase is 10. *Proc. Natl. Acad. Sci. U.S.A.* **98,** 4966–4971
9. Mitome, N., Suzuki, T., Hayashi, S., and Yoshida, M. (2004) Thermophilic ATP synthase has a decamer *c*-ring: indication of noninteger 10:3 H^+/ATP ratio and permissive elastic coupling. *Proc. Natl. Acad. Sci. U.S.A.* **101,** 12159–12164
10. Stahlberg, H., Müller, D. J., Suda, K., Fotiadis, D., Engel, A., Meier, T., Matthey, U., and Dimroth, P. (2001) Bacterial Na^+-ATP synthase has an undecameric rotor. *EMBO Rep.* **2,** 229–233
11. Meier, T., Matthey, U., von Ballmoos, C., Vonck, J., Krug von Nidda, T., Kühlbrandt, W., and Dimroth, P. (2003) Evidence for structural integrity in the undecameric *c*-rings isolated from sodium ATP synthases. *J. Mol. Biol.* **325,** 389–397
12. Pogoryelov, D., Yu, J., Meier, T., Vonck, J., Dimroth, P., and Muller, D. J. (2005) The c_{15}-ring of the *Spirulina platensis* F-ATP synthase: F_1/F_0 symmetry mismatch is not obligatory. *EMBO Rep.* **6,** 1040–1044
13. Meier, T., Ferguson, S. A., Cook, G. M., Dimroth, P., and Vonck, J. (2006) Structural investigations of the membrane-embedded rotor ring of the F-ATPase from *Clostridium paradoxum*. *J. Bacteriol.* **188,** 7759–7764
14. Meier, T., Morgner, N., Matthies, D., Pogoryelov, D., Keis, S., Cook, G. M., Dimroth, P., and Brutschy, B. (2007) A tridecameric *c*-ring of the adenosine triphosphate (ATP) synthase from the thermoalkaliphilic *Bacillus* sp. strain TA2.A1 facilitates ATP synthesis at low electrochemical proton potential. *Mol. Microbiol.* **65,** 1181–1192
15. Pogoryelov, D., Reichen, C., Klyszejko, A. L., Brunisholz, R., Muller, D. J., Dimroth, P., and Meier, T. (2007) The oligomeric state of *c*-rings from cyanobacterial F-ATP synthases varies from 13 to 15. *J. Bacteriol.* **189,** 5895–5902
16. Dimroth, P., Wang, H., Grabe, M., and Oster, G. (1999) Energy transduction in the sodium F-ATPase of *Propionigenium modestum*. *Proc. Natl. Acad. Sci. U.S.A.* **96,** 4924–4929
17. Vik, S. B., Patterson, A. R., and Antonio, B. J. (1998) Insertion scanning mutagenesis of subunit a of the F_1F_0 ATP synthase near His^{245} and implications on gating of the proton channel. *J. Biol. Chem.* **273,** 16229–16234; Correction (1998) *J. Biol. Chem.* **273,** 22159
18. Angevine, C. M., and Fillingame, R. H. (2003) Aqueous access channels in subunit *a* of rotary ATP synthase. *J. Biol. Chem.* **278,** 6066–6074
19. Angevine, C. M., Herold, K. A., and Fillingame, R. H. (2003) Aqueous access pathways in subunit *a* of rotary ATP synthase extend to both sides of the membrane. *Proc. Natl. Acad. Sci. U.S.A.* **100,** 13179–13183
20. Schwem, B. E., and Fillingame, R. H. (2006) Cross-linking between helices within subunit *a* of *Escherichia coli* ATP synthase defines the transmembrane packing of a four-helix bundle. *J. Biol. Chem.* **281,** 37861–37867
21. Angevine, C. M., Herold, K. A., Vincent, O. D., and Fillingame, R. H. (2007) Aqueous access pathway in ATP synthase subunit *a*: reactivity of cysteine substituted into transmembrane helices 1, 3, and 5. *J. Biol. Chem.* **282,** 9001–9007
22. Dong, H., and Fillingame, R. H. (2010) Chemical reactivities of cysteine substitutions in subunit *a* of ATP synthase define residues gating H^+ transport from each side of the membrane. *J. Biol. Chem.* **285,** 39811–39818
23. Börsch, M., Diez, M., Zimmermann, B., Reuter, R., and Gräber, P. (2002) Stepwise rotation of the γ-subunit of EF_0F_1-ATP synthase observed by intramolecular single-molecule fluorescence resonance energy transfer. *FEBS Lett.* **527,** 147–152
24. Düser, M. G., Zarrabi, N., Cipriano, D. J., Ernst, S., Glick, G. D., Dunn, S. D., and Börsch, M. (2009) 36° step size of proton-driven *c*-ring rotation in F_oF_1-ATP synthase. *EMBO J.* **28,** 2689–2696
25. Ishmukhametov, R., Hornung, T., Spetzler, D., and Frasch, W. D. (2010) Direct observation of stepped proteolipid ring rotation in *E. coli* F_oF_1-ATP synthase. *EMBO J.* **29,** 3911–3923
26. Junge, W., Lill, H., and Engelbrecht, S. (1997) ATP synthase: an electrochemical transducer with rotatory mechanics. *Trends Biochem. Sci.* **22,** 420–423
27. Moore, K. J., Angevine, C. M., Vincent, O. D., Schwem, B. E., and Fillingame, R. H. (2008) The cytoplasmic loops of subunit *a* of *Escherichia coli* ATP synthase may participate in the proton translocating mechanism. *J. Biol. Chem.* **283,** 13044–13052
28. Steed, P. R., and Fillingame, R. H. (2008) Subunit *a* facilitates aqueous access to a membrane-embedded region of subunit *c* in *Escherichia coli* F_1F_0 ATP synthase. *J. Biol. Chem.* **283,** 12365–12372
29. Steed, P. R., and Fillingame, R. H. (2009) Aqueous accessibility to the transmembrane regions of subunit *c* of the *Escherichia coli* F_1F_0 ATP synthase. *J. Biol. Chem.* **284,** 23243–23250
30. Cain, B. D., and Simoni, R. D. (1989) Proton translocation by the F_1F_0-ATPase of *Escherichia coli*: mutagenic analysis of the *a* subunit. *J. Biol. Chem.* **264,** 3292–3300
31. Hatch, L. P., Cox, G. B., and Howitt, S. M. (1995) The essential arginine residue at position 210 in the *a* subunit of the *Escherichia coli* ATP synthase can be transferred to position 252 with partial retention of activity. *J. Biol. Chem.* **270,** 29407–29412
32. Valiyaveetil, F. I., and Fillingame, R. H. (1997) On the role of Arg-210 and Glu-219 of subunit *a* in proton translocation by the *Escherichia coli* F_0F_1-ATP synthase. *J. Biol. Chem.* **272,** 32635–32641
33. Langemeyer, L., and Engelbrecht, S. (2007) Essential arginine in subunit *a* and aspartate in subunit *c* of F_oF_1 ATP synthase: effect of repositioning with helix 4 of subunit a and helix 2 of subunit *c*. *BBA-Bioenergetics* **1767,** 998–1005
34. Ishmukhametov, R. R., Pond, J. B., Al-Huqail, A., Galkin, M. A., and Vik, S. B. (2008) ATP synthesis without R210 of subunit *a* in the *Escherichia coli* ATP synthase. *Biochim. Biophys. Acta.* **1777,** 32–38
35. Mitome, N., Ono, S., Sato, H., Suzuki, T., Sone, N., and Yoshida, M. (2010) Essential arginine residue of the F_0-*a* subunit in F_0F_1-ATP synthase has a role to prevent the proton shortcut without *c*-ring rotation in the F_0 proton channel. *Biochem. J.* **430,** 171–177
36. Miller, M. J., Oldenburg, M., and Fillingame, R. H. (1990) The essential carboxyl group in subunit *c* of the F_1F_0 ATP synthase can be moved and H^+ translocating function retained. *Proc. Natl. Acad. Sci. U.S.A.* **87,** 4900–4904
37. Lomize, M. A., Lomize, A. L., Pogozheva, I. D., and Mosberg, H. I. (2006) OPM: orientations of proteins in membranes database. *Bioinformatics* **22,** 623–625

38. Rosso, L., and Gould, I. R. (2008) Structure and dynamics of phospholipid bilayers using recently developed general all-atom force fields. *J. Comput. Chem.* **29,** 24–37
39. Meier, T., Matthey, U., Henzen, F., Dimroth, P., and Müller, D. J. (2001) The central plug in the reconstituted undecameric c cylinder of a bacterial ATP synthase consists of phospholipids. *FEBS Lett.* **505,** 353–356
40. Emsley, P., Lohkamp, B., Scott, W. G., and Cowtan, K. (2010) Features and development of *Coot*. *Acta Crystallogr. D Biol. Crystallogr.* **66,** 486–501
41. Case, D. A., Cheatham, T. E., 3rd, Darden, T., Gohlke, H., Luo, R., Merz, K. M., Jr., Onufriev, A., Simmerling, C., Wang, B., and Woods, R. J. (2005) The Amber biomolecular simulation programs. *J. Comput. Chem.* **26,** 1668–1688
42. Cornell, W. D., Cieplak, P., Bayly, C. I., Gould, I. R., Merz, K. M., Ferguson, D. M., Spellmeyer, D. C., Fox, T., Caldwell, J. W., and Kollman, P. A. (1995) A second generation force field for the simulation of proteins, nucleic acids, and organic molecules. *J. Am. Chem. Soc.* **117,** 5179–5197
43. Simmerling, C., Strockbine, B., and Roitberg, A. E. (2002) All-atom structure prediction and folding simulations of a stable protein. *J. Am. Chem. Soc.* **124,** 11258–11259
44. Jorgensen, W. L., Chandrasekhar, J., Madura, J. D., Impey, R. W., and Klein, M. L. (1983) Comparison of simple potential functions for simulating liquid water. *J. Chem. Phys.* **79,** 926–935
45. Wang, J., Wolf, R. M., Caldwell, J. W., Kollman, P. A., and Case, D. A. (2004) Development and testing of a general amber force field. *J. Comput. Chem.* **25,** 1157–1174; Correction (2004) *J. Comput. Chem.* **26,** 114
46. Bayly, C. I., Cieplak, P., Cornell, W. D., and Kollman, P. A. (1993) A well-behaved electrostatic potential based method using charge restraints for deriving atom charges: the RESP model. *J. Phys. Chem.* **97,** 10269–10280
47. Tieleman, D. P., Marrink, S. J., and Berendsen, H. J. (1997) A computer perspective of membranes: molecular dynamics studies of lipid bilayer systems. *Biochim. Biophys. Acta* **1331,** 235–270
48. Anézo, C., de Vries, A. H., Höltje, H.-D., Tieleman, D. P., and Marrink, S.-J. (2003) Methodological issues in lipid bilayer simulations. *J. Phys. Chem. B* **107,** 9424–9433
49. Darden, T., York, D., and Pedersen, L. (1993) Particle mesh Ewald: an $N \cdot \log(N)$ method for Ewald sums in large systems. *J. Chem. Phys.* **98,** 10089–10092
50. Ryckaert, J.-P., Ciccotti, G., and Berendsen, H. J. (1977) Numerical integration of the Cartesian equations of motion of a system with constraints: molecular dynamics of *n*-alkanes. *J. Comput. Phys.* **23,** 327–341
51. Berendsen, H. J. C., Postma, J. P. M., van Gunsteren, W. F., DiNola, A., and Haak, J. R. (1984) Molecular dynamics with coupling to an external bath. *J. Chem. Phys.* **81,** 3684–3690
52. Suhre, K., and Sanejouand, Y. H. (2004) ElNémo: a normal mode web server for protein movement analysis and the generation of templates for molecular replacement. *Nucleic Acids Res.* **32,** W610–W614
53. Hakulinen, J. K., Klyszejko, A. L., Hoffmann, J., Eckhardt-Strelau, L., Brutschy, B., Vonck, J., and Meier, T. (2012) Structural study on the architecture of the bacterial ATP synthase F_o motor. *Proc. Natl. Acad. Sci. U.S.A.* **109,** E2050–E2056
54. Pogoryelov, D., Yildiz, O., Faraldo-Gómez, J. D., and Meier, T. (2009) High-resolution structure of the rotor ring of a proton-dependent ATP synthase. *Nat. Struct. Mol. Biol.* **16,** 1068–1073
55. Symersky, J., Pagadala, V., Osowski, D., Krah, A., Meier, T., Faraldo-Gómez, J. D., and Mueller, D. M. (2012) Structure of the c_{10}-ring of the yeast mitochondrial ATP synthase in the open conformation. *Nat. Struct. Mol. Biol.* **19,** 485–491
56. Lovell, S. C., Word, J. M., Richardson, J. S., and Richardson, D. C. (2000) The penultimate rotamer library. *Proteins* **40,** 389–408
57. Lau, W. C., and Rubinstein, J. L. (2012) Subnanometre-resolution structure of the intact *Thermus thermophilus* H^+-driven ATP synthase. *Nature* **481,** 214–218
58. Valiyaveetil, F. I., and Fillingame, R. H. (1998) Transmembrane topography of subunit *a* in the *Escherichia coli* F_1F_0 ATP synthase. *J. Biol. Chem.* **273,** 16241–16247
59. Long, J. C., Wang, S., and Vik, S. B. (1998) Membrane topology of subunit *a* of the F_1F_0 ATP synthase as determined by labeling of unique cysteine residues. *J. Biol. Chem.* **273,** 16235–16240
60. Meier, T., Polzer, P., Diederichs, K., Welte, W., and Dimroth, P. (2005) Structure of the rotor ring of F-type Na^+-ATPase from *Ilyobacter tartaricus*. *Science* **308,** 659–662
61. Krah, A., Pogoryelov, D., Meier, T., and Faraldo-Gómez, J. D. (2010) On the structure of the proton-binding site in the F_o rotor of chloroplast ATP synthases. *J. Mol. Biol.* **395,** 20–27
62. Pogoryelov, D., Krah, A., Langer, J. D., Yildiz, Ö., Faraldo-Gómez, J. D., and Meier, T. (2010) Microscopic rotary mechanism of ion translocation in the F_o complex of ATP synthases. *Nat. Chem. Biol.* **6,** 891–899
63. Jiang, W., and Fillingame, R. H. (1998) Interacting helical faces of subunits *a* and *c* in the F_1F_o-ATP synthase of *Escherichia coli* defined by disulfide cross-linking. *Proc. Natl. Acad. Sci. U.S.A.* **95,** 6607–6612
64. Dmitriev, O. Y., Freedman, K. H., Hermolin, J., and Fillingame, R. H. (2008) Interaction of transmembrane helices in ATP synthase subunit *a* in solution as revealed by spin label difference NMR. *BBA-Bioenergetics* **1777,** 227–237
65. Pierson, H. E., Uhlemann, E. M., and Dmitriev, O. Y. (2011) Interaction with monomeric subunit *c* drives insertion of ATP synthase subunit *a* into the membrane and primes *a-c* complex formation. *J. Biol. Chem.* **286,** 38583–38591
66. Zhang, D., and Vik, S. B. (2003) Close proximity of a cytoplasmic loop of subunit *a* with *c* subunits of the ATP synthase from *Escherichia coli*. *J. Biol. Chem.* **278,** 12319–12324
67. Groth, G. (2002) Structure of spinach chloroplast F_1-ATPase complexed with the phytopathogenic inhibitor tentoxin. *Proc. Natl. Acad. Sci. U.S.A.* **99,** 3464–3468